Estimating Watershed Evapotranspiration with PASS. Part I: Inferring Root-Zone Moisture Conditions Using Satellite Data

J. SONG

Department of Geography, Northern Illinois University, DeKalb, Illinois

M. L. WESELY AND R. L. COULTER

Environmental Research Division, Argonne National Laboratory, Argonne, Illinois

E. A. BRANDES

Research Applications Program, National Center for Atmospheric Research, Boulder, Colorado

(Manuscript received 27 August 1999, in final form 3 July 2000)

ABSTRACT

A model framework for parameterized subgrid-scale surface fluxes (PASS) has been modified and applied as PASS1 to use satellite data, models, and limited surface observations to infer root-zone available moisture (RAM) content with high spatial resolution over large terrestrial areas. Data collected during the 1997 Cooperative Atmosphere–Surface Exchange Study field campaign at the Atmospheric Boundary Layer Experiments site in the Walnut River watershed in Kansas were used to evaluate applications of the PASS1 approach to infer soil moisture content at times of satellite overpasses during cloudless conditions. Data from Advanced Very High Resolution Radiometers on the *NOAA-14* satellite were collected and then adjusted for atmospheric effects by using LOWTRAN7 and local atmospheric profile data from radiosondes. The input variables for PASS1 consisted of normalized difference vegetation index and surface radiant temperature, together with representative observations of downwelling solar irradiance, air temperature, relative humidity, and wind speed. Surface parameters, including roughness length, albedo, surface conductance for water vapor, and the ratio of soil heat flux to net radiation, were estimated with parameterizations suitable for the area using satellite data and land-use information; pixel-specific near-surface meteorological conditions such as air temperature, vapor pressure, and wind speed were adjusted according to local surface forcing; and RAM content was estimated using surface energy balance and aerodynamic methods. Comparisons with radar cumulative precipitation observations and in situ soil moisture estimates indicated that the spatial and temporal variations of RAM at the times of satellite overpasses were simulated reasonably well by PASS1.

1. Introduction

Soil moisture near the surface interacts strongly with the atmosphere through evapotranspiration and precipitation. The availability of soil moisture for evapotranspiration controls the partitioning between surface sensible and latent heat fluxes and is a major factor in controlling surface temperature. Because the sensible and latent heat fluxes strongly affect the structure of the planetary boundary layer (PBL), simulations of PBL behavior should take into account the spatial and temporal variation in soil moisture content.

Field observations of soil moisture content typically are too limited to provide the spatial resolution and coverage required to adequately describe the spatial heterogeneity of soil moisture over extended areas. Song et al. (1997) modeled the influence of heterogeneous soil moisture on latent and sensible heat fluxes and found that simulated regional-scale latent heat fluxes tend to be higher and air temperatures lower under uniform surface conditions than under spatially heterogeneous conditions. Pitman et al. (1993) demonstrated that possible biases associated with the underrepresentation of regional land surface heterogeneity within climate models might explain the propensity of climate models to overestimate grid-cell evapotranspiration and underestimate runoff. Hence, detailed information on the spatial distribution of the surface conditions appears to be necessary to simulate evapotranspiration accurately over extended areas.

A logical source of information related to spatial–temporal variation in land surface properties is remotely sensed data (e.g., Choudhury 1991). Various studies

Corresponding author address: Jie Song, Department of Geography, Northern Illinois University, DeKalb, IL 60115.
E-mail: jsong@geog.niu.edu

have shown that surface temperature estimated from space can be used to infer soil moisture (e.g., Ottlé and Vidal-Madjar 1994; Feddes et al. 1993). Recent analyses of surface soil moisture determined remotely from multispectral (thermal and vegetation index) measurements showed a wide range of surface radiant temperatures and vegetation fractions (Price 1990; Moran et al. 1994; Diak et al. 1995; Carlson et al. 1995; Gillies and Carlson 1995; Gillies et al. 1997), an observation that translates into a wide range of surface wetness. Gillies and Carlson (1995) and Moran et al. (1994) used the recognizable triangular shape of the pixel envelope in the scatterplot of the normalized difference vegetation index (NDVI) versus surface radiant temperature to estimate surface soil moisture. However, these methods can fall short because of uncertainties introduced by small-scale variations in air temperature, wind speed, roughness, and other surface and meteorological variables that influence soil moisture estimates. For example, soil water content derived with the triangle method versus that from soil hydrology models can show poor agreement on a pixel-by-pixel basis. The linear correlation between remotely derived soil water content and values derived with a soil hydrology model typically improve when averages are made over larger areas (Perry and Carlson 1988; Gillies et al. 1997).

Gillies et al. (1997) used an inversion procedure for multispectral data collected from aircraft to estimate surface moisture availability, fractional vegetation cover, and instantaneous surface energy fluxes. The procedure required the fitting of a measured variable to a simulated one, such that their equivalence defined a solution (e.g., for soil water content or surface energy fluxes). In this type of inversion, in which one or more parameters need to be obtained from measured values, a solution is obtained from model simulations rather than from a direct evaluation of a simple integral or function.

In general, techniques relying only on surface temperatures such as those inferred from infrared remote sensing usually do not provide accurate estimates of the profiles of moisture content in the soil. The surface soil tends to be drier than the layers below, and the ability of vegetation to extract moisture from various depths can confound relationships between the temperature of vegetative canopies and soil moisture at any one depth (e.g., Capehart and Carlson 1997). Although remote detection of soil moisture content in the upper 10 cm is possible with the use of passive microwave sensing at frequencies of about 1–18 GHz, factors like aboveground vegetative canopy biomass, surface roughness, soil texture, and soil organic matter content also affect the measured microwave brightness temperatures or polarization signals (e.g., Mattikalli et al. 1998; Vinnikov et al. 1999).

The parameterized subgrid-scale surface flux model (PASS) overcomes some of these limitations (Gao 1995; Gao et al. 1998). It couples Advanced Very High Resolution Radiometer (AVHRR) satellite data at individual pixels with limited meteorological observations in the study region to infer the root-zone available moisture (RAM) content for each pixel. The original PASS model has now been modified, refined, and separated into two parts. PASS1 is limited to inferring conditions near the times of satellite overpasses. PASS2 carries the simulation forward in time. This paper describes the use of PASS1 to infer RAM content at the Walnut River watershed (WRW) in southeastern Kansas.

2. Description of the PASS1 Model

The model grid (MG) size of many weather and climate models is about 100 km or larger, while satellite pixels and land use parcels with dimensions on the order of 0.01–1 km are on the subgrid (SG) scale. Routine surface meteorological observations are rarely made at locations consistently less than 100 km apart in large regions and thus are most suitable for MG applications. The PASS1 model uses existing surface observations and connects MG to SG processes with a simplified treatment of the surface energy balance of a plant–soil system. This approach uses (i) algorithms employing high-resolution satellite remote sensing data to derive the essential parameters for individual types of surfaces over large areas, (ii) methods to describe the interactions of near-surface atmospheric conditions with surface processes, and (iii) algorithms to compute RAM content at scales of satellite pixels or finer land use units. Figure 1 provides an outline of the approach. Values of SG surface parameters, including roughness length, surface albedo, surface conductance for water vapor, and the ratio of soil heat flux to net radiation, are estimated by using functional relationships between the surface parameters and satellite-derived spectral indices according to land-use classes. These relationships contain empirical coefficients whose values in this study had been derived for midlatitude areas with surface vegetation dominated by grasslands and agricultural crops and might not be suitable for areas with different surface characteristics. Pixel-specific near-surface meteorological conditions such as air temperature, vapor pressure, and wind speed are adjusted according to local surface forcing to account for the feedback of the locally influenced meteorological conditions on the local atmosphere–surface exchange. Values of RAM content at the SG level are then estimated by using surface energy budget and aerodynamic methods. The details of PASS1 can be considered in six steps (Fig. 1), which are accomplished without iteration except for a second pass starting at step 3, which involves the spatial distribution of ambient water vapor pressure.

a. Step 1, model inputs

The PASS1 model requires the provision of both MG and SG information. At the MG scale, observations are needed on incident solar radiation $\overline{K}\downarrow$, surface layer air temperature $\overline{T}_a$, relative humidity $\overline{\mathrm{RH}}$, and wind speed

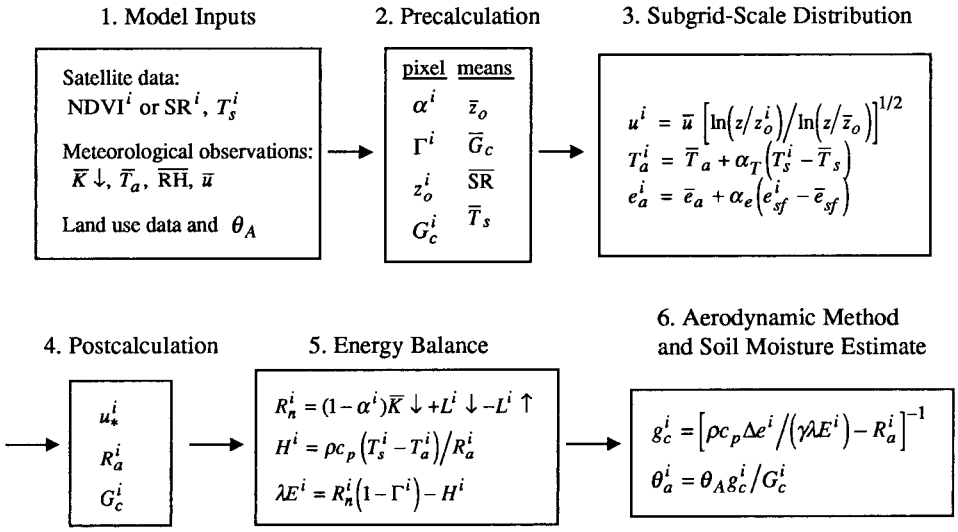

FIG. 1. Scheme of PASS1 model.

$\overline{u}$ at the time of the satellite overpass. The quantities $\overline{T}_a$, $\overline{\mathrm{RH}}$, and $\overline{u}$ are routinely measured as part of national and state networks of surface meteorological stations, and $\overline{K}\downarrow$ is often measured by special programs or state networks. In addition, $\overline{K}\downarrow$ could be calculated via retrievals of satellite data, for example, from Visible and Infrared Spin Scan Radiometers on Geostationary Operational Environmental Satellites (Gautier and Landsfeld 1997). At the SG scale, pixel-scale satellite information consisting of NDVI^i or the simple ratio SR^i and surface temperature T_s^i under cloudless skies is needed for each pixel *i.* Reflectances in the red waveband (AVHRR channel 1) and the near-infrared waveband (AVHRR channel 2) can be used to evaluate NDVI (ch2 − ch1)/(ch2 + ch1) and SR (ch2/ch1), and thermal radiances detected in AVHRR channels 4 and 5 can be converted to radiant temperature. Land-use data and root-zone available water capacity (θ_A) values are also necessary. In this study, the AVHRR data had a resolution of about 1 km. Calculations were made for 200-m pixels, conforming to the resolution of the datasets used on land use and root-zone available water capacity.

Surface temperature is a key variable in PASS1 calculations. The assumption is that the values of T_s^i derived from the satellite observations are good estimates of both the aerodynamic surface temperature and a temperature highly indicative of the evapotranspirative status of the vegetation as affected by soil moisture conditions in the root zone. This assumption is not always valid, especially for vegetative canopies that are not uniform or have locally variable coverage of the ground (e.g., woodlands in the WRW). In addition, the thermal radiance detected at the satellite can sometimes change systematically with view angle for agricultural row crops that do not entirely cover the ground. This type of crop coverage existed mostly at some of the winter wheat fields at the WRW for the period of time addressed in the present study. The effects of varying satellite view angles are ignored in this work. Finally, in the current PASS1, a surface emissivity of 0.98 is assumed for all surfaces. This value is typical of vegetation within a standard deviation of about 0.01 (Ottlé and Stoll 1993), which corresponds to an error of less than 1.5 K in surface temperature.

b. Step 2, precalculation

The surface parameters of canopy and surface resistance, aerodynamic resistance, surface albedo, and ratio of soil heat flux to net radiation are related to the spectral vegetation indices for each land use category. The vegetation indices are derived from satellite-based remote sensing of surface reflectances. Effectively quantifying these surface parameters at the satellite pixel scale is an important step in subgrid-scale surface parameterization. Use of satellite data, combined with appropriate surface interpretation algorithms and land-use data, provides descriptions of seasonal and annual changes in the amount and biophysical status of terrestrial vegetation at fine resolution.

1) ALBEDO

Albedo α varies with surface conditions and solar zenith angle. For vegetated land, α is found by using the parameterization described by Gao et al. (1998), based on calculations with a canopy reflectance model (Gao 1995):

$$\alpha^i = \alpha_0 + a_1 \exp\left(-\frac{a_2}{\mathrm{SR}^{i2}} - \frac{K}{\cos Z}\right). \qquad (1)$$

Here Z is the solar zenith angle, and α_0, a_1, a_2, and K are empirical coefficients (Table 1). For urban areas, a typical

TABLE 1. Surface albedo corresponding to the land use.

Land use	Albedo	α_0	α_1	α_2	K
Urban	0.15				
Cropland		0.10	0.14	6.08	0.25
Rangeland		0.25	−0.14	6.08	0.25
Woodland		0.10	0.14	6.08	0.25
Water	$-0.0139 + 0.0467 \tan Z$ $1 \geq \alpha \geq 0.03$				

TABLE 2. Roughness length corresponding to land use.

Land-use category	Roughness length (m)
Urban	0.7
Cropland	$10^{-3.02+2.22\text{NDVI}}$
Rangeland	$10^{-3.02+2.27\text{NDVI}}$
Woodland	1
Water	0.0001

value of $\alpha^i = 0.15$ is assumed (e.g., Landsberg 1981; Oke 1987). For water, α^i is a function of solar zenith angle, as shown in Table 1 (e.g., Atwater and Ball 1981).

2) RATIO OF SOIL HEAT FLUX TO NET RADIATION

The ratio of soil heat flux to net radiation Γ^i for vegetated surfaces is found as a function of SR^i and Z, as described by Gao et al. (1998):

$$\Gamma^i = \frac{\mu_1}{(\text{SR}^i)^{\mu_2}} \exp\left(-\frac{K}{\cos Z}\right). \quad (2)$$

Here the empirical coefficients μ_1, μ_2, and K are 0.539, 0.4, and 0.25, respectively; and Z is restricted to values smaller than 88°. The influence of soil moisture on the ground heat flux is ignored in this version of PASS1. For urban areas, Γ^i is assumed to be equal to 0.3, a relatively large value to account for the heat storage of buildings. A value of 0.3 is used here for open water, a rough approximation that has little impact because open water exists in the WRW in only very limited areas of rivers and reservoirs.

3) SURFACE ROUGHNESS

Estimates of surface roughness length (z_0^i) on pixel-sized scales are based on land-use data and NDVI, which considers both permanent land cover and seasonal changes. Typical values of z_0 for urban, woodland, and water surfaces have been given by Stull (1988) and various other sources in the scientific literature. We assume a value of $z_0 = 0.7$ m for the fairly open urban areas found in Great Plains cities, a value slightly smaller than that found in some urban areas (Grimmond et al. 1998). Woodland areas consist mainly of groves and trees along streams, and a value of $z_0 = 1$ m is chosen. Values of z_0 for fairly uniform surfaces typical of agricultural fields in the WRW croplands and woodlands vary from 0.07 to 0.13h, where h is canopy height (e.g., Garratt 1992). Here we select $z_0 = 0.1h$ and find h with formulations based on field observations made above wheat and grass in northern Illinois (J. Song 1998, unpublished manuscript). Table 2 summarizes the roughness length values and calculations for the five dominant land-use categories in the WRW.

For each SG pixel, z_0^i is the roughness length. The average roughness value $\overline{z}_0$ for the entire MG region is computed as

$$\overline{z}_0 = (z_r - d) \exp\left\{\frac{1}{n}\sum_{i=1}^{n}\left[\ln\left(\frac{z_0^i}{z_r - d}\right)\right]^{-1}\right\}^{-1}. \quad (3)$$

Here where z_r represents the reference height, about 10 m above the aerodynamic displacement height d, which for vegetation is roughly two-thirds of the canopy height. This formulation is one of several that could be used (e.g., André and Blondin 1986; Vihma and Savijärvi 1991) and was chosen in part because of its compatibility with the distribution function described later for wind speed.

4) SURFACE CONDUCTANCE

The procedure described by Gao (1995) is used to find the total surface conductance g_c^i for water vapor. The conductance is found as the product of the conductance G_c^i for unstressed vegetation and the extraction function f_2, which accounts for the constraint by RAM and is explained in step 6. Evaluation of G_c^i incorporates the conductance G_0 for nonvegetated surfaces or senescent canopies and vegetative factors associated with photosynthetically active radiation (PAR, estimated as $0.5\overline{K}\downarrow$), SR^i, and the atmospheric water vapor deficit δe^i. In precalculations, the atmospheric water vapor deficit for each pixel is set to be the mean from the surface meteorological observations in the MG region. The soil water content is initially unknown, so G_c^i for saturated soil conditions is first calculated instead of g_c^i:

$$G_c^i = G_0 + \frac{\beta_1 \text{PAR}}{(\beta_2 + \text{PAR})}(\text{SR}^i - \text{SR}_0) f_1(\delta e^i). \quad (4)$$

Here the factor $f_1 = (1 + \beta_3 \delta e)^{-1}$ describes the influence on the surface conductance by the atmospheric water vapor deficit δe (Kim and Verma 1991). The empirical coefficients used in the above expressions are $\beta_1 = 0.285 \times 10^{-2}$ m s^{-1}, $\beta_2 = 156$ W m^{-2}, and $\beta_3 = 0.093$ kPa^{-1}. Here SR_0 is the simple ratio for nonvegetated surfaces or those with senescent vegetation. If SR^i is less than SR_0, then G_c^i is set equal to G_0. For urban areas, the surface conductance G_0 is small; it is assumed to be zero in PASS1.

c. Step 3, subgrid-scale distribution

The regional meteorological variables for wind speed, air temperature, and water vapor pressure are spatially distributed to individual pixels according to the surface

conditions and strength of the local vertical transfer. In PASS1, the distribution functions that relate wind speed $\overline{u}$ to u^i, air temperature $\overline{T}_a$ to T_a^i, and atmospheric vapor pressure $\overline{e}_a$ to e_a^i are

$$u^i = \overline{u}\left[\ln\left(\frac{z_r - d}{z_0^i}\right)\Big/\ln\left(\frac{z_r - d}{\overline{z}_0}\right)\right]^{1/2}, \quad (5)$$

$$T_a^i = \overline{T}_a + \alpha_T(T_s^i - \overline{T}_s), \quad (6)$$

$$e_a^i = \overline{e}_a + \alpha_e(e_{\rm sf}^i - \overline{e}_{\rm sf}). \quad (7)$$

Here the overbars denote an average over the MG region. The distribution function for wind is based on the approximation that uu_* at a reference height of about 10 m above the aerodynamic displacement height is invariant for a given set of atmospheric conditions (e.g., Walcek et al. 1986). Equation (5) is theoretically consistent with computing $\overline{u}$ by means of a logarithmic profile equation using $\overline{z}_0$ from Eq. (3) and a regional friction velocity found from the arithmetic mean of the momentum fluxes across the area. Because the friction velocities are not routinely measured at surface meteorological stations, $\overline{u}$ is found here from the arithmetic mean of wind speeds observed at the sites in the region and an adjustment with an expression similar to Eq. (5) to account for the domain-average surface roughness versus the average surface roughness at the observational sites. The numerical coefficients α_T and α_e represent the strength of surface forcing, which is affected by turbulent mixing processes within the atmospheric boundary. In the current PASS1, both α_T and α_e are set at 0.57, according to a previous study for similar terrain and vegetation (Gao 1995). The surface temperature T_s^i is obtained from satellite thermal channels. The vapor pressure $e_{\rm sf}$ of the air effectively in contact with the canopy or land bulk surface is estimated from the following relationship:

$$e_{\rm sf}^i = e_{\rm sat}^i(T_s^i) - E^i R_v T_a^i / g_c^i. \quad (8)$$

Here $e_{\rm sat}(T_s)$ is the surface saturation vapor pressure, E^i is the turbulent moisture flux, and R_v is water vapor gas constant. Tests conducted with PASS1 have shown that an alternative method of recalculating the vapor pressure distribution, based on root-zone moisture content instead of surface vapor pressure in Eq. (7) (Gao 1995; Seth et al. 1994), produces almost the same results as does Eq. (7). PASS1 uses surface vapor pressure in Eq. (7) because it describes physical processes similar to those indicated by Eq. (6); thus, the coefficients α_e and α_T are more likely to have the same value, as is assumed in PASS1.

Because E^i and g_c^i are both unknown quantities initially, a temporary substitute for Eq. (7) is needed for a single iteration through steps 3–6. Tests have shown that additional iterations are not necessary. The surface conductances from step 2 are used for this substitution, in the following equation:

$$e_a^i = \overline{e}_a\left[1 + \alpha_e\left(\frac{G_c^i - \overline{G}_c}{\overline{G}_c}\right)\right]. \quad (9)$$

d. Step 4, postcalculation

The conductance G_c^i for vegetation that is not stressed by lack of moisture (which occurs when the soil is saturated or nearly saturated with water) is recalculated in step 4 using Eq. (4) with pixel-specific estimates of δe^i based on the SG values of T_a^i and e_a^i estimated from the distribution functions. Friction velocity u_*^i and aerodynamic resistance R_a^i are found with SG values of u^i estimated from the distribution function and roughness length z_0^i at individual pixels, as

$$u_*^i = 0.4u^i\left[\ln\left(\frac{z_r - d}{z_0^i}\right)\right]^{-1}, \quad (10)$$

$$R_a^i = \frac{1}{0.4u_*^i}\ln\left(\frac{z_{rT} - d}{z_{0h}^i}\right). \quad (11)$$

Here roughness length z_{0h} is related to z_0 by the expression $\ln(z_0/z_{0h}) \simeq 2$, which is appropriate for uniform surfaces but might not be adequate for incomplete vegetative canopies. The term z_{rT} denotes the reference heights at which temperature and humidity are observed, typically 1.5–2.0 m above the aerodynamic displacement height. Estimates of u_*^i and R_a^i made with Eqs. (10) and (11) could be modified to incorporate the effects of nonneutral conditions by using stability functions based on bulk Richardson numbers computed with the values of u^i, T_a^i, and T_s^i (e.g., as outlined by Zhang et al. 1995). As is noted in the discussion for step 5, however, use of stability corrections tends to produce inferior results with the present PASS1 configuration.

e. Step 5, surface energy balance

The surface radiation budget for each pixel is

$$R_n^i = (1 - \alpha^i)K\downarrow + L^i\downarrow - L^i\uparrow, \quad (12)$$

where $L^i\downarrow$ and $L^i\uparrow$ represent the incoming and outgoing longwave irradiances, respectively. The latter quantity is estimated from the Stefan–Boltzmann law and surface temperature T_s^i. The downward irradiance is parameterized as a function of air temperature and vapor pressure according to Satterlund (1979):

$$L^i\downarrow = 1.08\sigma T_a^{i4}[1 - \exp(-e_a^{iT_a^i/2016})]. \quad (13)$$

Here σ is the Stefan–Boltzmann constant, e_a^i is vapor pressure in millibars, and T_a^i is atmospheric temperature in Kelvin.

The sensible heat flux H^i for each pixel is estimated from the temperature difference between air and surface by using the aerodynamic expression

$$H^i = \frac{\rho^i c_p}{R_a^i}(T_s^i - T_a^i). \quad (14)$$

Here ρ^i is the air density and c_p is the specific heat of air at constant pressure. The latent heat flux λE^i is then calculated as the residual term in the surface energy balance:

$$\lambda E^i = R_n^i(1 - \Gamma^i) - H^i. \quad (15)$$

This method of estimating the latent heat flux as a residual quantity of the surface energy balance is necessary because the surface resistance is not yet estimated at this step of the calculations. One disadvantage of this method is that poor estimates of R_a^i can result in significant errors in λE^i. For example, tests conducted with PASS1 with its use of Eq. (5) as a distribution function for wind speed have indicated that using stability adjustments for u_*^i and R_a^i in step 4 sometimes results in unreliable estimates of R_a^i for daytime conditions, which can cause excessively large values of H^i and small values of λE^i. Thus, stability adjustments have not been applied for the simulations described in this paper, which conforms with Gao's (1995) practice of not using them in earlier versions of the PASS model. Another example is that the present version of PASS1 tends to produce unusually small values of R_a^i for the large roughness length of woodlands, increasing H^i and decreasing λE^i excessively. This tendency results from the limitations in the distribution functions for isolated or relatively rare surfaces whose properties differ greatly from the average. To consider such surfaces, which include reservoirs, rivers, and woodlands in the WRW, observations of wind speed over these specific types of surfaces ideally would be used, but such measurements were not made for this study. In addition, surface radiometric temperature might consistently overestimate surface temperature for the incomplete canopies that dominate woodlands in the WRW, in which case underestimates of R_a^i would lead to unusually large values of H^i. Woodlands occur mostly along rivers in the WRW and cover a very small portion of the domain, so the present version of PASS1 sets the value of R_a^i for the woodland land-use class equal to an average value for the domain.

f. Step 6, root-zone available moisture

The RAM content (θ_a) is found as a function of the soil moisture extraction function f_2, which is calculated in PASS1 as the ratio g_c^i/G_c^i (Fig. 1). The surface conductance is calculated as $g_c^i = 1/R_c^i$, where R_c^i is found via the following aerodynamic relationship:

$$\lambda E^i = \frac{\rho^i C_p}{\gamma(R_a^i + R_c^i)}[e_{\text{sat}}^i(T_s^i) - e_a^i]. \quad (16)$$

Here γ is the psychrometric constant.

Using θ_a is a slight deviation from the approach used in previous versions of PASS that rely on relative available soil moisture content (Gao 1995; Gao et al. 1998). The RAM content θ_a is defined as the difference between the absolute moisture content θ and the wilting point moisture content θ_w; all three quantities are the volumetric fraction expressed in centimeter per centimeter of soil or $m^3\ m^{-3}$ of soil. The amount of moisture represented by θ_a is the portion of the available soil moisture capacity θ_A that exists at a particular time. Because θ_A is the difference between field capacity moisture content θ_f and θ_w, θ_a determines the amount of soil moisture that influences evapotranspiration rate. Previous studies have typically used either a linear or a nonlinear dependence of f_2 on soil moisture content.

TABLE 3. Soil moisture properties for several soil textures, derived from Buckman and Brady (1960) and, in parentheses, from Rutter (1975).

	θ_f	θ_w	θ_A
Sandy loam	(0.27)	(0.11)	(0.16)
Loam	0.21 (0.34)	0.10 (0.13)	0.11 (0.21)
Silt loam	0.28 (0.38)	0.12 (0.14)	0.16 (0.24)
Clay loam	0.29 (0.30)	0.13 (0.16)	0.15 (0.14)
Clay	0.30 (0.39)	0.16 (0.22)	0.14 (0.17)

Betts et al. (1997) conducted sensitivity tests using both linear and nonlinear relationships in numerical models and found that linear relationships tended to produce more realistic variations in soil moisture content with time in some situations. The independent variable can be defined as $\Theta = \theta_a/\theta_A$ and the linear relationship as (e.g., Mahfouf and Noilhan 1991)

$$f_2 = \Theta. \quad (17)$$

An advantage to this approach is that θ_A can be used directly without knowledge of θ_f or θ_w; databases on θ_A for the United States are available from the U.S. Department of Agriculture (SSURGO 1995).

Many types of nonlinear formulations have been developed to describe the relationships between terms equivalent to f_2 and measures of soil moisture (e.g., see Brutsaert 1982; Abramopoulos et al. 1988). The nonlinear relationships sometimes include fairly precise descriptions of the relationships between moisture content and water potential in the soil (e.g., Fuentes et al. 1992). The nonlinear function examined here requires estimates of θ_f and θ_w. Although the concepts of field capacity and wilting point are essential for many practical applications, the corresponding values reported vary considerably. Table 3 summarizes some representative values for these quantities. The values without parentheses are derived from Buckman and Brady (1960) as summarized by Oke (1987), and the values in parentheses are derived from information summarized by Rutter (1975). The degree of compaction and amount of soil organic matter probably accounts for some of the variability.

We assume that the wilting point corresponds to a soil suction value of $\Psi_w = 15$ bar and the saturation corresponds to a soil suction of 0.2 bar. These assumptions allow a simple solution of the function $\Psi = a(\theta_a)^b$,

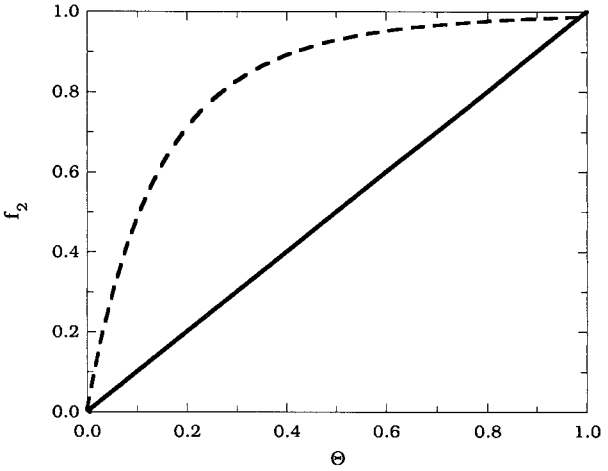

FIG. 2. Extraction function f_2 depicted as a linear and a nonlinear function of relative available soil moisture.

described by Hillel (1998) and based on the work of Gardner et al. (1970). The values of a and b can be calculated for the assumed soil moisture properties. The function f_2 can be related to the soil suction (e.g., Abramopoulos et al. 1988) as $f_2 = (\Psi_w - \Psi)/\Psi_w$. The available soil moisture content θ_a can be found as $\theta_a = \theta_w[(1 - f_2)^{-1/b} - 1]$.

Figure 2 shows f_2 versus relative available soil moisture Θ plotted for both the linear and nonlinear formulations. The nonlinear function allows less variation of evapotranspiration when the values of θ_a are fairly large and produces a steeper decrease of the availability of moisture for evapotranspiration as the soil dries. The sensitivity of this approach to wilting point estimates makes them susceptible during drydown to the effects of inaccuracies in estimates of soil moisture content and soil hydrological properties. Also, a disadvantage of the nonlinear relationship is that it requires knowledge of wilting point values, which are highly variable and not available in databases for large regions. In contrast, the linear function allows evapotranspiration to have a more even sensitivity to available moisture and requires only data on θ_A, which are readily available at fairly high spatial resolution (SSURGO 1995).

3. Application

Measurements of a wide range of surface and PBL conditions were made during April and May 1997 at the WRW by the Cooperative Atmosphere–Surface Exchange Study (CASES) consortium and the Atmospheric Boundary Layer Experiments (ABLE) facility operated by Argonne National Laboratory (LeMone et al. 2000). The WRW covers an area of approximately 5000 km^2 east of Wichita, Kansas. It is located in the Arkansas–Red River basin and is enclosed by the southern Great Plains Clouds and Radiation Testbed of the U.S. Department of Energy's Atmospheric Radiation Measurement (ARM) program. Figure 3 shows the spatial distribution of the observation sites in the WRW. The 1997 CASES campaign and routine ABLE operations provided surface-based observations of the vertical profiles of temperature, relative humidity, and wind, as well as the air–surface exchange rates of heat, moisture, and momentum. One of the objectives of CASES-97 was to document the effects of surface wetness on PBL structure. As variations in precipitation, surface vegetation, and thus soil moisture content occurred spatially and temporally in the WRW, it served as a testbed to assess the ability of PASS1 to couple satellite data with meteorological observation to characterize the variation of RAM content with high spatial resolution over large terrestrial areas.

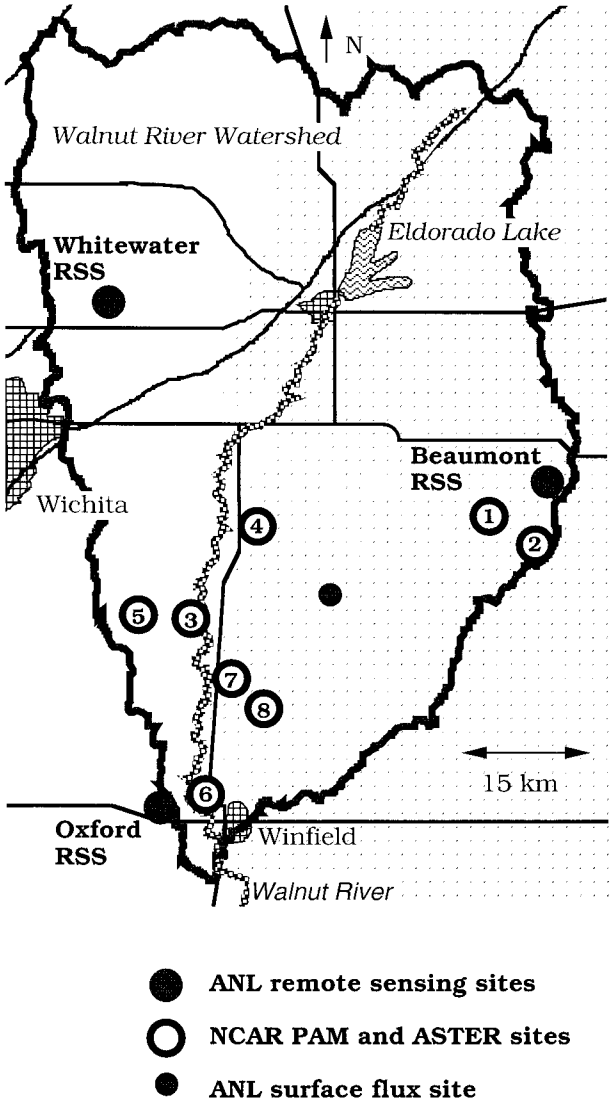

FIG. 3. Observation sites in the Walnut River Watershed (WRW). The type of surface vegetation at each of the eight NCAR sites is noted in Table 5.

TABLE 4. *NOAA-14* satellite overpass information and spatially averaged surface meteorological conditions.

DOY	Time (GMT)	Visibility (km)	$\overline{K}\downarrow$ (W m^{-2})	$\overline{T}_a$ (C)	$\overline{RH}$ (%)	$\overline{u}$ (m s^{-1})
119	20:07	90	886	26.0	32.5	9.6
130	19:47	120	945	20.7	29.2	5.2
140	19:38	110	953	20.6	42.7	5.0

a. Satellite data

In this study, the PASS1 analysis focused on three cloudless days in 1997: 29 April, 10 May, and 20 May [days of year (DOY) 119, 130, and 140]. The WRW had distinctive surface wetness patterns on each day because of the varying nature of previous precipitation events and the changing vegetation conditions as the ''greening'' of the surface progressed. The AVHRR satellite data noted in Table 4 were chosen in part because the overpass times of the satellite over the region occurred near midday. The satellite view angle varied from 4° to 44.5° on the three days, which has been taken into account in computing atmospheric corrections. With these views at the small solar zenith angles at the time of the satellite overpasses, the effects of bidirectional reflection on NDVI and SR observations could be assumed to be negligible. The AVHRR data were obtained by direct reception of the National Oceanic and Atmospheric Administration (NOAA) *NOAA-14* satellite high-resolution picture transmission (HRPT). The HRPT data used here cover an area within latitudes of 37.15°–38.17°N and longitudes of 96.47°–97.33°W. The size of each satellite pixel is approximately 1 km. The reflectances in the red waveband (channel 1, 0.58–0.68 μm) and near-infrared waveband (channel 2, 0.73–1.10 μm) were used to estimate NDVI and SR, and the radiances for channels 4 (10.5–11.5 μm) and 5 (11.5–12.5 μm) in the thermal infrared range were converted to radiant temperature by the standard procedure documented in the NOAA satellite user's manual (Kidwell 1998).

To derive ground-level spectral reflectances and surface temperature from the satellite-derived at-sensor values, calculations of atmospheric scattering, absorption, transmission, and emission in the layer from the satellite altitude to the altitude of the site were made with the commonly used atmospheric radiation transfer model LOWTRAN7, with radiosonde data obtained near the town of Oxford, Kansas, and values of visibility inferred from total extinction coefficient measurements with a nephelometer at the ARM central facility in north-central Oklahoma. The differences in reflectances between satellite-level values and corresponding ground-level values were estimated with the algorithm suggested by Fraser et al. (1992), which allowed the reflectances to be adjusted for atmospheric effects. The ground-level radiant temperature was obtained by adjusting the raw values with calculated atmospheric transmittance and radiance in the thermal region associated with AVHRR channels 4 and 5. Surface temperatures (T_s) were derived from the radiant temperatures with the assumption that the surface emissivity was equal to 0.98.

With reliable radiosonde data and local estimates of visibility, LOWTRAN7 appeared to make adequate atmospheric corrections for some of the days. A general limitation with this approach is that local visibility data of high quality are not always readily available. All visibility values greater than 10 miles (16.2 km) are reported as 10 miles by National Weather Service stations. On DOY 124 and 136, the readings at the ARM site, which is located about 100 km from the WRW, did not appear to be representative of the WRW, possibly because haze was not uniform over the region. Thus the satellite data from these two days were not used in this study. In general, the spatial variability of haze and other atmospheric conditions, including subvisual incipient clouds, tend to lessen the reliability of the adjustments.

The split-window method (Price 1984) might be an alternative to using LOWTRAN7 to adjust for the effects of the atmosphere on the derived values of surface temperature. The split-window technique has the advantage of not requiring independently derived estimates of atmospheric scattering and absorption, but its accuracy for land surfaces can be questioned (e.g., Gao et al. 1998). For DOY 119 and 130, the surface temperatures derived from the split-window technique were cooler by about 7.1° and 3.4°C, respectively, than those found with LOWTRAN7 for pixels for which the surface was entirely exposed water, primarily for Eldorado Lake in the northeast portion of the WRW. On DOY 140, surface temperatures derived from the split-window technique were about 2.1°C warmer than those found using LOWTRAN7 for the pixels representing Eldorado Lake. An adjustment as large as 7.1°C to the LOWTRAN7-derived surface temperatures for DOY 119 would have resulted in unrealistically large estimates of RAM. Use of a fraction of these differences to adjust the values of surface temperature derived using LOWTRAN7 might be feasible and was attempted in the present study. However, a justification for choosing a particular value for the fraction or other means of making adjustments using the split-window technique was not found. Thus, data from the split-window technique were not used in this study. Derivation of improved methods to evaluate the surface temperature remains the subject of future research.

The spatial and temporal patterns of NDVI and surface radiant temperature varied on the three different days. Values of NDVI were relatively small in the eastern grassland area on DOY 119 and 130. Larger values occurring over the whole WRW area on DOY 140 reflect the gradual springtime greening of the vegetation. The surface temperatures on DOY 119 and 130 were higher than on DOY 140, except for a few spots in the southwest on DOY 119 and patches of lower temperature in the northwest and southwest on DOY 130.

TABLE 5. Vegetative conditions at the eight NCAR sites.

Site 1: Grassland (minimal grazing)
Site 2: Grassland (minimal grazing)
Site 3: Bare ground planted to maize and soybeans
Site 4: Sparse grass (bare ground to south)
Site 5: Winter wheat
Site 6: Winter wheat on floodplain
Site 7: Winter wheat on south-facing slope
Site 8: Grassland (ungrazed)

b. Meteorological observations

During CASES-97, ABLE and the National Center for Atmospheric Research (NCAR) operated equipment at the WRW locations sketched in Fig. 3. Standard surface meteorological observations were made with automatic weather stations located at two ABLE remote sensing sites and the surface flux site near the town of Smileyberg. NCAR operated six Portable Automated Mesonet (PAM) stations and two Atmosphere-Surface Turbulent Exchange Research (ASTER) systems in the southern portion of the WRW to measure surface energy fluxes, near-surface soil moisture content and temperature, surface meteorological parameters, and related quantities. The estimates of $\overline{K}\downarrow$, $\overline{T}_a$, $\overline{\mathrm{RH}}$, and $\overline{u}$ needed as PASS1 input parameters were made from the arithmetic means of observations at the eight NCAR sites (Table 4). The vegetative conditions at each site are described in Table 5. Vertical profiles of temperature and humidity were obtained from radiosondes operated by NCAR near Oxford.

c. Land-use and surface hydrological data

Land-use classes for the WRW and the immediately surrounding area are displayed in Fig. 4 with a horizontal resolution of 200 m. The classes were derived from a dataset based on an unsupervised classification of Landsat Thematic Mapper data performed by the Kansas Applied Remote Sensing Program (DASC 1993). The original data files contained information with a resolution of 30 m, but a resolution of 200 m was considered adequate to isolate individual types of sur-

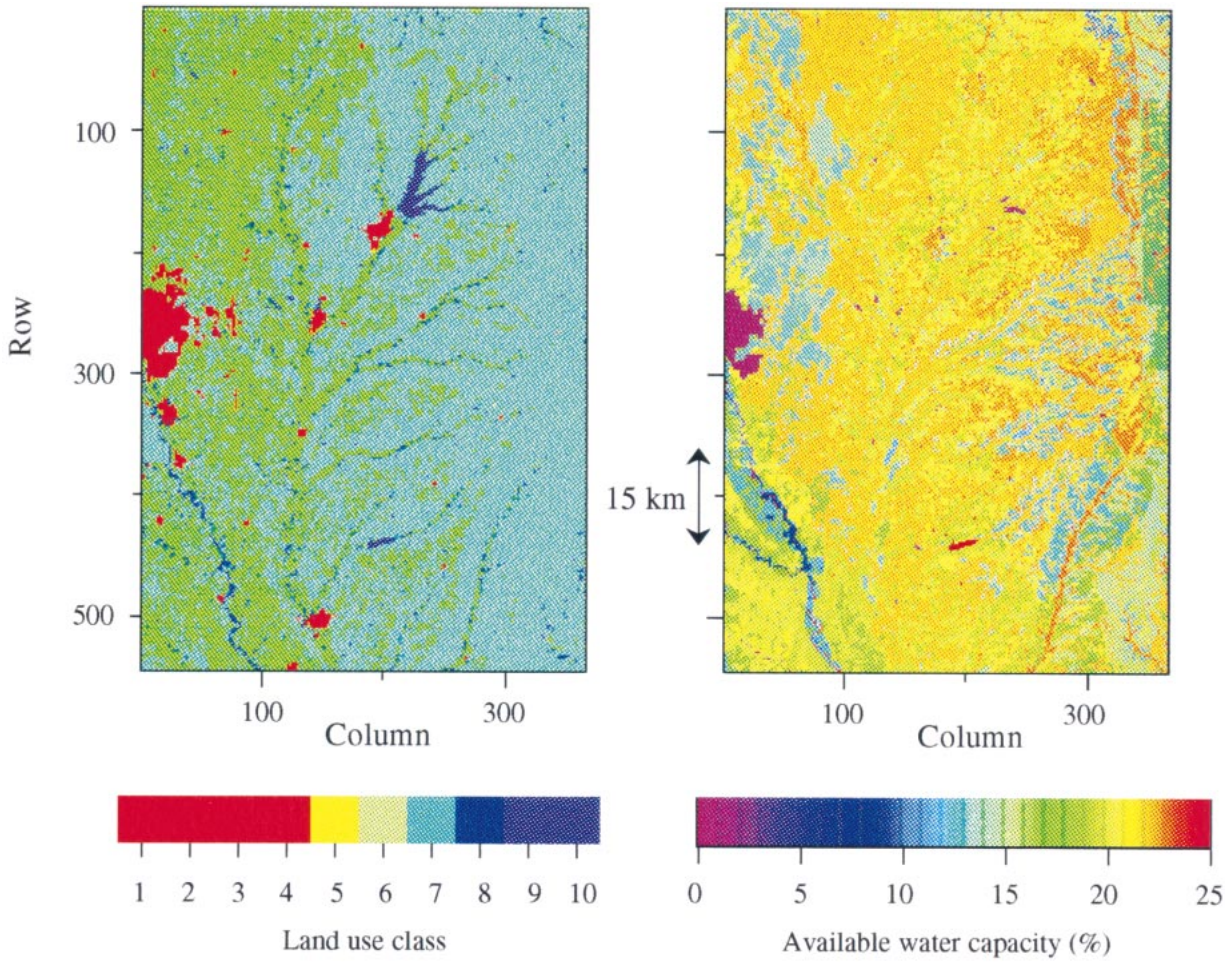

FIG. 4. Map (left) of land-use classes in the WRW (classes 1–5: urban land uses; 6: cropland; 7: rangeland; 8: woodland; 9: water; and 10: others); and map (right) of available water capacity in the top layer of soils in the WRW.

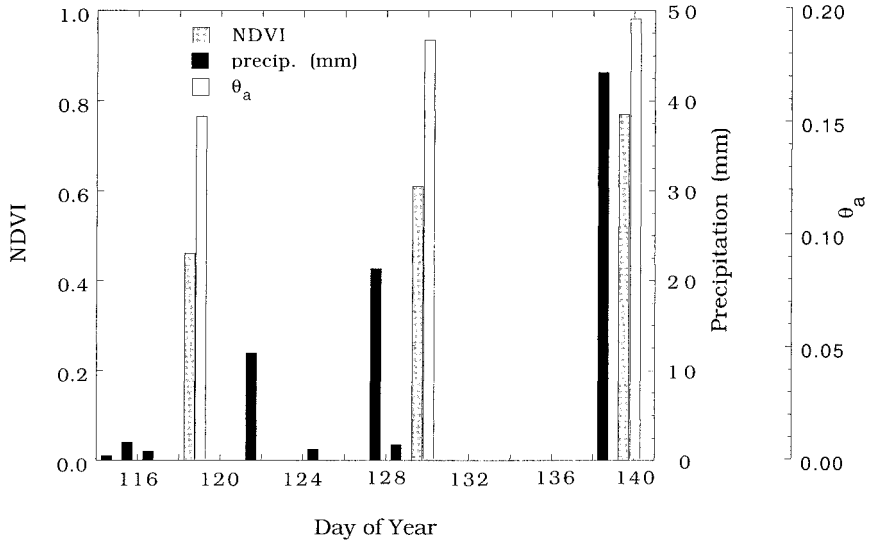

FIG. 5. Variation of measured precipitation at Wichita, KS, and domain-averaged estimates of RAM content (θ_a) and NDVI, in 1997.

faces in relation to the 1-km resolution of the NDVI data. As has already been described, the land-use data were applied to calculate roughness lengths, albedos, surface conductances, and ratio of ground heat flux to net radiation.

Data on available water capacity θ_A with 200-m resolution (Fig. 4) were extracted from datasets based on county soil survey manuals (SSURGO 1995). Estimates of neither θ_f nor θ_w are made during most county soil surveys; thus, the values are not readily available, hindering the application of nonlinear f_2 functions. For tests conducted with PASS1 to compare results of nonlinear versus linear versions of f_2, we assumed that θ_w was two-thirds of θ_A. This assumption is based on the typical values shown in Table 3 and the fact that the textural classes of soils in the WRW are mostly silt loam in the hills in the east and the central lowlands and silty clay loam on the western uplands (Penner et al. 1975).

4. Results and evaluation

a. Trends in precipitation, NDVI, and RAM content

Estimates of θ_a were made by using both the linear and nonlinear f_2 expressions for each 200-m resolution pixel at the times of the three chosen satellite overpasses. Figure 5 shows the values of whole-domain arithmetic mean of θ_a using the linear expression for f_2, as well as values of NDVI, in relation to precipitation amounts independently measured previously at a National Weather Service station in Wichita, Kansas. The domain, defined by the latitudes and longitudes given in section 3a, was roughly a rectangle that encompassed the WRW. The entire area was greening up during the experimental period, as is indicated by the trend in NDVI. The values of θ_a were clearly responding to the amounts of rainfall in the area. The averaged estimates of θ_a were 0.152, 0.186, and 0.195 for the linear function and 0.103, 0.167, and 0.195 for the nonlinear function on DOY 119, 130, and 140, respectively. The nonlinear f_2 thus produced significantly lower values of θ_a during dry (DOY 119) and moderately moist (DOY 130) soil conditions.

b. Comparison with spatial precipitation patterns

Figure 6 shows the spatial patterns in θ_a, derived from the linear f_2 function, along with event rainfall amounts independently derived from an S-band polarized radar system operated by NCAR at a location west of the WRW; the estimates of rainfall amounts were adjusted with data from a network of over 30 rain gauges operated by Oregon State University and other networks in the area (Brandes et al. 1999; LeMone et al. 2000). The horizontal patterns in θ_a changed with time in a manner evidently dependent on the antecedent precipitation fields. Scattered areas in the WRW received light precipitation on the 3–4 days prior to DOY 119 (for which a radar image was not available), as indicated by scattered areas of high RAM content in the southern WRW and the relatively dry soil conditions in the northern parts. With the rainfall received on DOY 122 and 127–128, the soil moisture on DOY 130 can be seen in Fig. 6 to have become fairly evenly distributed, except for dry conditions in the far southern portion of the WRW and slightly drier conditions near the center of the WRW in areas lying between the bands of rain during the event on DOY 127–128. On DOY 140, the variation of RAM content appears in Fig. 6 to largely mirror the distribution of θ_A, after the heavy rainfall that oc-

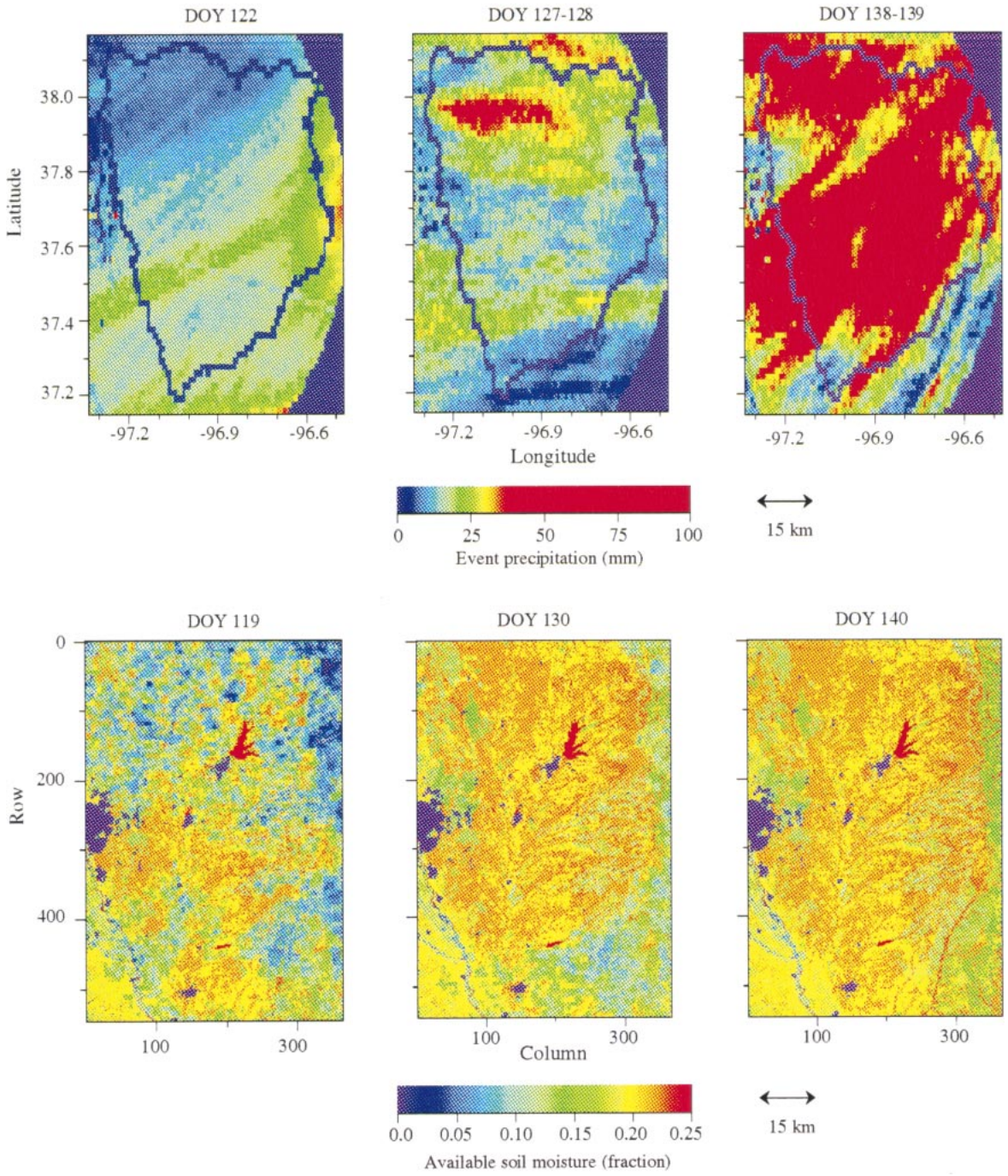

FIG. 6. Patterns of modeled RAM content and cumulative precipitation measured on selected days by radar during rain events.

curred on DOY 138 and 139. The spatial patterns (not shown) of θ_a derived from the nonlinear f_2 function were similar to the pattern for the linear relationship for DOY 140, but the former had excessively sharp spatial variations for DOY 119 and 130; the sharpness was induced by the nonlinear function when the soil is unsaturated.

c. Comparison with in situ soil moisture measurements

In situ soil moisture measurements were made at the eight NCAR sites in the southern WRW (Fig. 3) by using reflectometer probes placed across a depth of 1–9 cm in the soil, so that the readings were representative

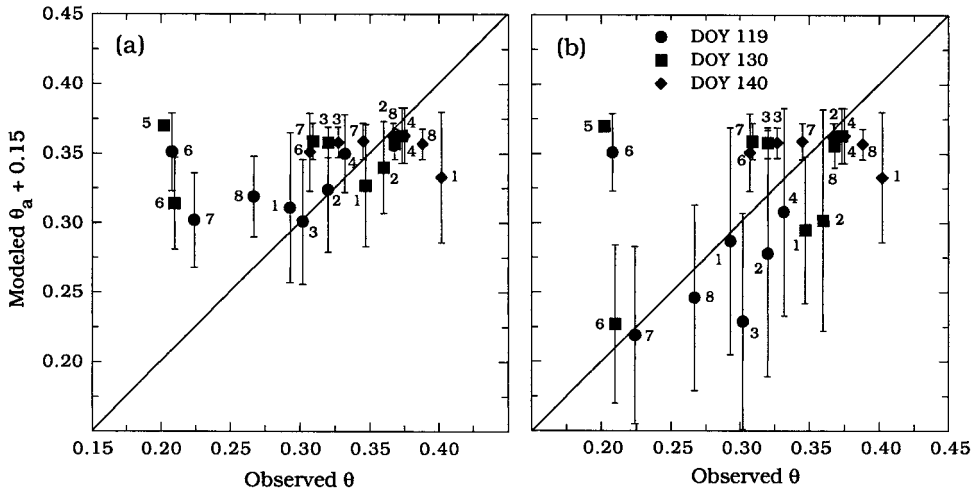

FIG. 7. Model results on RAM content (θ_a) for (a) linear f_2 and (b) nonlinear f_2 vs soil moisture (θ) measured at a depth of about 5 cm at the eight NCAR sites during CASES-97. The error bars indicate one standard deviation on each side of the model means for the pixels within about 1 km of the measurement sites.

of a depth of about 5 cm. Minor adjustments in the thermal response of the probes were applied to the soil moisture values provided by NCAR, to produce more realistic diurnal variations in the moisture content. In general, comparison of the local in situ measurements to the model estimates for individual pixels is difficult, in part because soil moisture content can vary significantly along fairly short horizontal distances. The current study used 200-m resolution pixels for land use and 1-km resolution data for NDVI and surface temperature; estimates of the latter two quantities were probably frequently affected by a mixture of contrasting surface conditions within one pixel, for example, bare soil and vegetation in adjacent fields. Furthermore, the geographic registration of the 1-km resolution satellite data was considered accurate only to within about one pixel. In an attempt to make some comparison, nevertheless, estimates of θ_a were averaged over all of the 200-m pixels within 1 km of each NCAR site. Figure 7 shows the means and standard deviations of the θ_a estimates for the 121 pixels that were centered as closely as possible on each measurement location. Data points on the straight lines would indicate perfect agreement only if the value of wilting point moisture content θ_w were exactly 0.15; values ranging at least from 0.13 to 0.17 are likely for the soils and vegetation at the sites. As expected, the variability of the data derived by using the nonlinear relationship (Fig. 7b) is usually larger than that of data from the linear relationship (Fig. 7a), especially for low levels of modeled RAM content.

The modeled RAM contents found with the linear relationship are slightly larger than the observations, which is more realistic than the most frequent case of underestimates obtained with the nonlinear relationship. The soil moisture in the root zone or deep soil layers is usually depleted more slowly than in the upper layer where the measurements were made. For example, a few, infrequent samples of soil moisture profiles indicated that the range of soil moisture content measured in the upper 10 cm of the soil in the wheat field of site 7 varied from 0.18 to 0.30 (for the dry conditions of DOY 118 and the wet conditions on DOY 141, respectively), from 0.27 to 0.30 at a depth of 25 cm, and from 0.44 to 0.46 at a depth of 50 cm. By comparison, the variations at the site 8 grassland were smaller: 0.24–0.35 in the upper 10 cm, 0.40–0.46 at 25 cm, and 0.46–0.48 at 50 cm.

The values of near-surface soil moisture content observed for the winter wheat fields at sites 5, 6, and 7 were consistently lower than for the grasslands or bare soil that existed at the other sites, except after heavy rainfall preceding DOY 140. Unusually small moisture contents were measured at site 5 on DOY 130 and site 6 on DOY 130. Also, the measurements of soil moisture profiles indicated that the moisture content increased rapidly with depth in the wheat field when the surface was dry. The difference in the moisture content across the upper 10 cm of the soil in the wheat field at site 7 was at least 0.10 in all but very moist conditions, while the gradient across the upper soil layer in the grassland site was usually less than 0.05. The typical small-scale horizontal variations that naturally occur in soil moisture, together with the strong vertical gradients and temporal variability of the soil moisture content seen in the upper 10 cm in the wheat field, suggests that the single probes used at sites 5 and 6 could have been placed in unrepresentative locations near the surface. When the data from site 5 on DOY 130 and site 6 on DOY 119 are included in a linear regression analysis, the resulting R value is 0.34 for the linear f_2 function and 0.42 for the nonlinear function. The R values increase to 0.65 and 0.75 for the linear and nonlinear functions, respec-

tively, when the two points are excluded. With these two points excluded, the arithmetic mean of the ratio of $\theta_a + 0.15$ to the observed values is 1.06 (with a standard deviation of 0.15) for the linear form of f_2 and 0.97 (with a standard deviation of 0.11) for the nonlinear form of f_2.

5. Conclusions

A new version of the parameterized subgrid-scale surface fluxes model (PASS1) was developed specifically for times of satellite overpasses to evaluate surface energy fluxes and the root-zone moisture content at satellite pixel scales over extended areas. As in previous versions of PASS, model inputs consist of standard surface meteorological observations, solar insolation data, and estimates of NDVI and thermal infrared temperature derived from satellite observations. Modeled values of RAM content (θ_a) plus a representative value of wilting point moisture content for the WRW agreed on average with observed soil moisture content during CASES-97 to within 6% for the mean, with a standard deviation of about 15%. Also, the pattern in θ_a matched rain gauge–corrected radar observations of previous rainfall events, and θ_a values computed for individual sites were similar to in situ data on soil moisture content measured in the upper soil layer at eight locations. These comparisons were limited to fairly moist conditions and to areas typical of the Great Plains.

PASS1 uses more physically realistic distribution functions for wind speed and ambient water vapor content than were used previously by PASS. For the ambient water vapor content, the distribution function using surface vapor pressure produces effectively the same results as a function using estimated RAM content. Future work might lead to a better distribution function for wind speed, for example, by considering atmospheric stability and roughness more explicitly. For woodlands, the current version of PASS1 produced poor estimates of aerodynamic resistance R_a unless the roughness length was reduced to unrealistically small values.

PASS1 incorporates a linear relationship between RAM content and the extraction factor that relates evapotranspiration rate without moisture stress to the rate with moisture stress. The linear function might be less satisfactory than a nonlinear relationship for individual sites with extensive soil characterization, but the linear relationship in PASS1 appears to produce more realistic spatial variations in soil moisture content. Furthermore, the linear relationship can be used with databases derived from soil surveys that estimate available water capacity.

This research is intended to lead to an operational version of PASS for use in evaluating evapotranspiration for hydrological studies. PASS1 is applied only for the time of satellite overpasses and is intended to provide initial data for using PASS2 for the time intervals between the overpasses. In addition, PASS1 has the potential of providing initialization and assimilation data on soil moisture content for weather forecast and possibly climate models, which is a desirable feature because dense networks of soil moisture measurement stations are generally not available as a data source.

The use of LOWTRAN7 to make atmospheric adjustments to infer the surface reflectances and infrared radiances from satellite data is a technique that could, in principle, be automated for routine applications. At least daily radiosonde data would be needed as well as measurements of optical depths or visibility in the area. The visibility data would have to be of higher quality, especially for large values of visibility, than those typically acquired at conventional surface meteorological stations. In addition, the horizontal variability of water vapor and aerosols in the atmosphere can lessen the accuracy of the atmospheric adjustments for a particular subgrid area in the modeling domain. Use of the split-window technique for open water in reservoirs and lake provides an alternative approach for various locations in the domain, although the split-window approach applied to bodies of open water in terrestrial surroundings was found to be unreliable in this study. Improved analytical or observational methods of inferring the surface optical radiances of large areas are needed, especially for infrared surface temperature.

Acknowledgments. This work was supported by the National Aeronautics and Space Agency Order S-10133-X directed to the U.S. Department of Energy. Work by Argonne National Laboratory to collect ABLE data during CASES-97 was supported by the U.S. Department of Energy, Office of Science, Office of Biological and Environmental Research, Environmental Science Division, under Contract W-31-109-Eng-38. Some of the analysis of CASES-97 data was supported by the U.S. Department of Energy's ARM program. Activities of the first author were funded in part by the National Science Foundation through Grant ATM 97-09948. The AVHRR data were collected with the guidance of Barry M. Lesht of Argonne. The land use and available water capacity information were obtained and assembled in suitable datasets by Alice T. Cialella of Brookhaven National Laboratory as part of her work for the U.S. Department of Energy's ARM program. Much of the rain gauge data used to adjust the rainfall estimates with the S-band polarized radar system during CASES-97 was supplied by Richard H. Cuenca and colleagues in the Department of Bioresource Engineering at Oregon State University. Data from the PAM stations and ASTER systems were provided by the Atmospheric Technology Division of NCAR.

REFERENCES

Abramopoulos, F., C. Rosenzweig, and B. Choudhury, 1988: Improved ground hydrology calculations for global climate models

(GCMs): Soil water movement and evapotranspiration. *J. Climate,* **1,** 921–941.

André, J.-C., and C. Blondin, 1986: On the effective roughness length for use in numerical three-dimensional models. *Bound.-Layer Meteor.,* **35,** 231–245.

Atwater, M. A., and J. T. Ball, 1981: A surface solar radiation model for cloudy atmospheres. *Mon. Wea. Rev.,* **109,** 878–888.

Betts, A., F. Chen, K. Mitchell, and Z. Janjić, 1997: Assessment of the land surface and boundary layer models in two operational versions of the NCEP Eta model using FIFE data. *Mon. Wea. Rev.,* **125,** 2896–2915.

Brandes, E. A., J. Vivekanandan, and J. W. Wilson, 1999: A comparison of radar reflectivity estimates of rainfall from collocated radars. *J. Atmos. Oceanic Technol.,* **16,** 1264–1272.

Brutsaert, W. H., 1982: *Evaporation into the Atmosphere. Theory, History, and Applications.* D. Reidel, 299 pp.

Buckman, H. O., and N. C. Brady, 1960: *The Nature and Properties of Soils.* Macmillan, 567 pp.

Capehart, W. J., and T. N. Carlson, 1997: Decoupling of surface and near-surface soil water content: A remote sensing perspective. *Water Resour. Res.,* **33,** 1383–1395.

Carlson, T. N., R. R. Gillies, and T. J. Schmugge, 1995: An interpretation of NDVI and radiant surface temperature as measures of surface soil water content and fractional vegetation cover. *Agric. For. Meteor.,* **77,** 191–205.

Choudhury, B. J., 1991: Multispectral satellite data in the context of land surface heat balance. *Rev. Geophys.,* **29,** 217–236.

DASC, cited 1993: Land cover. Data Access and Support Center, Kansas Geological Survey, University of Kansas, Lawrence, Kansas. [Available online at http://gisdasc.kgs.ukans.edu/dasc.html.]

Diak, G. R., R. M. Rabin, K. P. Gallo, and C. M. U. Neale, 1995: Regional-scale comparisons of vegetation and soil wetness with surface energy budget properties from satellite and in-situ observations. *Remote Sens. Rev.,* **12,** 355–382.

Feddes, R. A., M. Menenti, P. Kabat, and W. G. M. Bastiaanssen, 1993: Is large-scale inverse modelling of unsaturated flow with areal average evaporation and surface soil moisture as estimated from remote sensing feasible? *J. Hydrol.,* **143,** 125–152.

Fraser, R. S., R. A. Ferrare, Y. J. Kaufman, B. L. Markham, and S. Mattoo, 1992: Algorithm for atmospheric corrections of aircraft and satellite imagery. *Int. J. Remote Sens.,* **13,** 541–557.

Fuentes, C., R. Haverkamp, and J.-Y. Parlange, 1992: Parameter constraints on closed-form soilwater relationships. *J. Hydrol.,* **134,** 117–142.

Gao, W., 1995: Parameterization of subgrid-scale land surface fluxes with emphasis on distributing mean atmospheric forcing and using satellite-derived vegetation index. *J. Geophys. Res.,* **100,** 14 305–14 317.

——, R. L. Coulter, B. M. Lesht, J. Qiu, and M. L. Wesely, 1998: Estimating clear-sky regional surface fluxes in the southern Great Plains Atmospheric Radiation Measurement site with ground measurements and satellite observations. *J. Appl. Meteor.,* **37,** 5–22.

Gardner, W. R., D. Hillel, and Y. Benyamini, 1970: Post irrigation movement of soil water: I. Redistribution. *Water Resour. Res.,* **6,** 851–861.

Garratt, J. R., 1992: *The Atmospheric Boundary Layer.* Cambridge University Press, 316 pp.

Gautier, C., and M. Landsfeld, 1997: Surface solar radiation flux and cloud radiative forcing for the Atmospheric Radiation Measurement (ARM) Southern Great Plains (SGP): A satellite, surface observations, and radiative transfer model study. *J. Atmos. Sci.,* **54,** 1289–1307.

Gillies, R. R., and T. N. Carlson, 1995: Thermal remote sensing of surface soil water content with partial vegetation cover for incorporation into climate models. *J. Appl. Meteor.,* **34,** 745–756.

——, ——, J. Cui, W. P. Kustas, and K. S. Humes, 1997: A verification of the triangle method for obtaining surface soil water content and energy fluxes from remote measurements of the normalized difference vegetation index (NDVI) and surface radiant temperature. *Int. J. Remote Sens.,* **18,** 3145–3166.

Grimmond, C. S. B., T. S. King, M. Roth, and T. R. Oke, 1998: Aerodynamic roughness of urban areas derived from wind observations. *Bound.-Layer Meteor.,* **89,** 1–24.

Hillel, D., 1998: *Environmental Soil Physics.* Academic Press, 771 pp.

Kidwell, K. B., cited 1998: NOAA Polar Orbiter data user's guide. National Climatic Data Center, National Oceanic and Atmospheric Administration, Washington, DC. [Available online at http://www2.ncdc.noaa.gov/docs/podug/.]

Kim, J., and S. B. Verma, 1991: Modeling canopy conductance in a temperate grassland ecosystem. *Agric. For. Meteor.,* **55,** 149–166.

Landsberg, H. E., 1981: *The Urban Climate.* Academic Press, 275 pp.

LeMone, M. A., and Coauthors, 2000: Land–atmosphere interaction research and opportunities in the Walnut River Watershed in southeast Kansas: CASES and ABLE. *Bull. Amer. Meteor. Soc.,* **81,** 757–779.

Mahfouf, J. F., and J. Noilhan, 1991: Comparative study of various formulations of evaporation from bare soil using in situ data. *J. Appl. Meteor.,* **30,** 1354–1365.

Mattikalli, N. M., E. T. Engman, T. J. Jackson, and L. R. Ahuja, 1998: Microwave remote sensing of temporal variations of brightness temperature and near-surface soil water content during a watershed-scale field experiment, and its application to the estimation of soil physical properties. *Water Resour. Res.,* **34,** 2289–2299.

Moran, M. S., T. R. Clarke, Y. Inoue, and A. Vidal, 1994: Estimating crop water deficit using the relation between surface-air temperature and spectral vegetation index. *Remote Sens. Environ.,* **49,** 246–263.

Oke, T. R., 1987: *Boundary Layer Climates.* Methuen and Company, 435 pp.

Ottlé, C., and M. Stoll, 1993: Effect of atmospheric absorption and surface emissivity on the determination of land surface temperature from infrared satellite data. *Int. J. Remote Sens.,* **14,** 2025–2037.

——, and D. Vidal-Madjar, 1994: Assimilation of soil moisture inferred from infrared remote sensing in a hydrological model over the HAPEX-MOBILHY region. *J. Hydrol.,* **158,** 241–264.

Penner, H. L., S. C. Ekart, D. A. Eqing, G. Schmidt, and J. Smith, 1975: Soil survey of Butler County, Kansas. U.S. Department of Agriculture Soil Conservation Service and Kansas Agricultural Experiment Station, 60 pp. [Available from State Conservationist, 760 South Broadway, Salina, KS 67401.]

Perry, E. M., and T. N. Carlson, 1988: Comparison of active microwave soil water content with infrared surface temperatures and surface moisture availability. *Water Resour. Res.,* **24,** 1818–1824.

Pitman, A. J., Z. L. Yang, and A. Henderson-Sellers, 1993: Subgrid scale precipitation in AGCMs: Re-assessing the land surface sensitivity using a single column model. *Climate Dyn.,* **9,** 33–41.

Price, J. C., 1984: Land surface temperature measurements from the split-window channels of NOAA 7 advanced very high resolution radiometer. *J. Geophys. Res.,* **89,** 7231–7237.

——, 1990: Using spatial context in satellite data to infer regional scale evapotranspiration. *IEEE Trans. Geosci. Remote Sens.,* **28,** 940–948.

Rutter, A. J., 1975: The hydrological cycle in vegetation. *Vegetation and the Atmosphere,* Vol. 1, *Principles,* J. L. Monteith, Ed., Academic Press, 111–154.

Satterlund, D. R., 1979: An improved equation for estimating longwave radiation from the atmosphere. *Water Resour. Res.,* **15,** 1649–1650.

Seth, A., F. Giorgi, and R. E. Dickinson, 1994: Simulating fluxes from heterogeneous land surfaces: Explicit subgrid method employing the biosphere-atmosphere transfer scheme (BATS). *J. Geophys. Res.,* **99,** 18 651–18 667.

Song, J., C. J. Willmott, and B. Hanson, 1997: Influence of hetero-

geneous land surfaces on surface energy and mass fluxes. *Theor. Appl. Climatol.*, **58,** 175–188.

SSURGO, 1995: Soil Survey Geographic (SSURGO) data base. U.S. Department of Agriculture, 31 pp. [Available from National Cartography and GIS Center, USDA, National Resources Conservation Service, P.O. Box 6567, Fort Worth, TX 76115.]

Stull, R. B., 1988: *An Introduction to Boundary Layer Meteorology*. Kluwer Academic, 666 pp.

Vihma, T., and H. Savijörvi., 1991: On the effective roughness length for heterogeneous terrain. *Quart. J. Roy. Meteor. Soc.*, **117,** 399–407.

Vinnikov, K. Y., A. Robock, S. Qiu, J. K. Entin, M. Owe, B. J. Choudhury, S. E. Hollinger, and E. G. Nyoku, 1999: Satellite remote sensing of soil moisture in Illinois, United States. *J. Geophys. Res.*, **104,** 4145–4168.

Walcek, C. J., R. A. Brost, J. S. Chang, and M. L. Wesely, 1986: SO_2, sulfate and HNO_3 deposition velocities computed using regional landuse and meteorological data. *Atmos. Environ.*, **20,** 949–964.

Zhang, L., R. Lemeur, and J. P. Goutorbe, 1995: A one-layer resistance model for estimating regional evapotranspiration using remote sensing data. *Agric. For. Meteor.*, **77,** 241–261.